UC Davis
UC Davis Previously Published Works

Title

A transient, closed-loop network of wireless, body-integrated devices for autonomous electrotherapy.

Permalink

https://escholarship.org/uc/item/387971d5

Journal

Science, 376(6596)

Authors

Choi, Yeon
Yin, Rose
Avila, Raudel
et al.

Publication Date

2022-05-27

DOI

10.1126/science.abm1703

Peer reviewed

A transient, closed-loop network of wireless, body-integrated devices for autonomous electrotherapy

Yeon Sik Choi[1,2,22,†], **Hyoyoung Jeong**[1,2,†], **Rose T. Yin**[3,†], **Raudel Avila**[8], **Anna Pfenniger**[4], **Jaeyoung Yoo**[1,2], **Jong Yoon Lee**[1,2,7], **Andreas Tzavelis**[1,2,5,6], **Young Joong Lee**[1,2], **Sheena W. Chen**[9,10], **Helen S. Knight**[3], **Seungyeob Kim**[1,2,11], **Hak-Young Ahn**[1,2,22], **Grace Wickerson**[1,2,12], **Abraham Vázquez-Guardado**[1,2], **Elizabeth Higbee-Dempsey**[13], **Bender A. Russo**[3], **Michael A. Napolitano**[9,10], **Timothy J. Holleran**[9,10], **Leen Abdul Razzak**[1,2,5], **Alana N. Miniovich**[3], **Geumbee Lee**[1,2], **Beth Geist**[4], **Brandon Kim**[7], **Shuling Han**[14,15], **Jaclyn A. Brennan**[3], **Kedar Aras**[3], **Sung Soo Kwak**[1,2,23], **Joohee Kim**[1,2], **Emily Alexandria Waters**[5,18], **Xiangxing Yang**[16], **Amy Burrell**[4], **Keum San Chun**[16], **Claire Liu**[1,2,3], **Changsheng Wu**[1,2], **Alina Y. Rwei**[17], **Alisha N. Spann**[18], **Anthony Banks**[1,2], **David Johnson**[4], **Zheng Jenny Zhang**[14,15], **Chad R. Haney**[5,18], **Sung Hun Jin**[1,2,11], **Alan Varteres Sahakian**[5,19], **Yonggang Huang**[1,3,8,20], **Gregory D. Trachiotis**[10], **Bradley P. Knight**[4], **Rishi K. Arora**[4,*], **Igor R. Efimov**[2,3,*], **John A. Rogers**[1,2,5,8,12,21,*]

[1]Center for Bio-Integrated Electronics, Northwestern University, Evanston, IL 60208, USA.

[2]Querrey Simpson Institute for Bioelectronics, Northwestern University, Evanston, IL 60208, USA.

[3]Department of Biomedical Engineering, The George Washington University, Washington, DC 20052, USA.

[4]Feinberg School of Medicine, Cardiology, Northwestern University, Chicago, IL 60611, USA.

[5]Department of Biomedical Engineering, Northwestern University, Evanston, IL 60208, USA.

[6]Medical Scientist Training Program, Feinberg School of Medicine, Northwestern University, Chicago, IL 60611, USA.

[7]Sibel Health, Niles, IL, 60714, USA.

[8]Department of Mechanical Engineering, Northwestern University, Evanston, IL 60208, USA.

[9]Department of General Surgery, The George Washington University, Washington, DC 20052, USA.

[10]Department of Cardiothoracic Surgery, Veteran Affairs Medical Center, Washington, DC 20422, USA.

[11]Department of Electronic Engineering, Incheon National University, 119 Academy-ro, Yeonsu-gu, Incheon, 406-772, Republic of Korea.

[12]Department of Materials Science and Engineering, Northwestern University, Evanston, IL 60208, USA.

[13]Developmental Therapeutics Core, Northwestern University, Evanston, IL 60208, USA.

[14]Comprehensive Transplant Center, Feinberg School of Medicine, Northwestern University, Chicago, IL 60611, USA.

[15]Department of Surgery, Feinberg School of Medicine, Northwestern University, Chicago, IL 60611, USA.

[16]Department of Electrical and Computer Engineering, University of Texas at Austin, Austin, Tx, 78712, USA.

[17]Department of Chemical Engineering, Delft University of Technology, Van der Maasweg 9, 2629 HZ Delft, The Netherlands.

[18]Center for Advanced Molecular Imaging, Northwestern University, Evanston, IL 60208, USA.

[19]Department of Electrical and Computer Engineering, Northwestern University, Evanston, IL 60208, USA.

[20]Department of Civil and Environmental Engineering, Northwestern University, Evanston, IL 60208, USA.

[21]Department of Neurological Surgery, Feinberg School of Medicine, Northwestern University, Chicago, IL 60611, USA.

[22]Precision Biology Research Center, Sungkyunkwan University, Suwon, 16419, Republic of Korea.

[23]Current Address: Center for Bionics of Biomedical Research Institute, Korea Institute of Science and Technology, Seoul 02792, Korea

Abstract

Temporary post-operative cardiac pacing requires devices with percutaneous leads and external wired power and control systems. This hardware introduces risks for infection, limitations on patient mobility, and requirements for surgical extraction procedures. Bioresorbable pacemakers mitigate some these disadvantages, but they demand pairing with external, wired systems and secondary mechanisms for control. We present a transient closed-loop system that combines a time-synchronized, wireless network of skin-integrated devices with an advanced bioresorbable pacemaker to control cardiac rhythms, track cardiopulmonary status, provide multi-haptic feedback, and enable transient operation with minimal patient burden. The result provides a range of autonomous, rate-adaptive cardiac pacing capabilities, as demonstrated in rat, canine, and human heart studies. This work establishes an engineering framework for closed-loop temporary electrotherapy using wirelessly linked, body-integrated bioelectronic devices.

One-Sentence Summary:

A closed-loop network of body-integrated wireless devices enables rate-adaptive temporary cardiac pacing

---

All living systems function through the interaction of complex networks of physiological feedback loops to maintain homeostasis. Engineering approaches to treat disorders, such as cardiac pacemakers, exploit conceptually similar methods for closed-loop control to enable autonomous, adaptive regulation of one or more essential physiological parameters to target set points, without human intervention (1-3). These and other existing platforms have key limitations that follow from their reliance on conventional electronic hardware, monitoring schemes and interfaces to the body. First, these systems often require physical tethers and percutaneous access points that may lead to systemic infections (4-7). Second, connections to external modules for power supply, sensing, control, and other essential functions constrain the mobility of the patients and impede clinical care. Third, removal or replacement of electronic components (e.g. leads and batteries) demand surgical procedures that impose additional risks and burdens on patients (8, 9). These features can extend durations of hospitalizations, often in intensive care units. For example, short-term bradyarrhythmias that commonly occur in the 5-7 days after cardiac surgery must be treated with temporary transcutaneous pacing systems, typically prolonging hospital stays with limited ability to initiate physical therapy (Supplementary Text 1). Recently reported wireless, bioresorbable medical implants for temporary therapies address some of these challenges, they still require external, wall-plugged equipment for monitoring, power and control (10-16).

This paper introduces a transient, closed-loop system that incorporates a time-synchronized, wireless network with seven key components: (i) a temporary, bioresorbable, stretchable epicardial pacemaker; (ii) a bioresorbable steroid-eluting interface that minimizes local inflammation and fibrosis (17); (iii) a subcutaneous, bioresorbable power harvesting unit; (iv) a set of soft, skin-interfaced sensors that capture electrocardiograms (ECGs), heart rate (HR), respiratory information, physical activity, and cerebral hemodynamics for physiological monitoring of the patient; (v) a wireless radiofrequency (RF) module that transfers power to the harvesting unit; (vi) a soft, skin-interfaced haptic actuator that communicates via mechanical vibrations; and (vii) a handheld device with a software application for real-time visualization, storage, and analysis of data for automated adaptive control. These components integrate into a fully implantable, bioresorbable module (i-iii), a set of skin-interfaced modules (iv-vi), and an external control module (vii). Fig. 1A illustrates the use of this system for temporary cardiac pacing. The bioresorbable module wirelessly receives power for epicardial pacing. A network of skin-interfaced modules transmits diverse physiological data to the control module via Bluetooth Low Energy (BLE) protocols for real-time data visualization and algorithmic control. A haptic module provides tactile feedback to the patient. After a period of therapy, the bioresorbable module dissolves in the body, and the skin-interfaced modules are removed by peeling off the skin. These 'transient' characteristics of the system eliminate the need for surgical removal and allow ambulatory end of treatment. Fig. 1B illustrates the closed-loop scheme that interconnects

these modules into a wireless network (table S1). Soft, flexible designs (Fig. 1C) enable placement of the modules onto various target locations of the body.

Fig. 1D shows that the constituent materials of the bioresorbable module completely disappear in simulated biofluid consisting of phosphate-buffered saline (PBS). Results of in vivo studies are in fig. S1. This module consists of an RF power harvester, which includes an inductive receiver (Rx) coil (molybdenum, Mo) and a RF PIN diode (silicon nanomembrane, Si NM), a pair of stretchable interconnects (Mo), and stimulation electrodes that integrate a steroid eluting patch at the myocardial interface (Fig. 2A). The thin, lightweight, and stretchable design minimizes the possibility for infection, with geometries that can be tailored to the anatomy of the patient (fig. S2). Fig. 2B shows scattering parameters (S_{11}) of power harvesters with three different sizes of Rx coils (Supplementary Text 2). Continuous alternating current applied to a transmission (Tx) coil wirelessly delivers power to the Rx coil via magnetic induction and induces an approximately direct current monophasic output defined by the diode rectifier (Fig. 2C). The magnetic resonance imaging (MRI) compatibility of this wireless system is discussed in Supplementary Text 3. Top and bottom encapsulating layers of a bioresorbable dynamic covalent polyurethane (b-DCPU) and stretchable electrodes (11) ensure reliable pacing against the mechanically dynamic surface of the heart (18). Fig. 2D shows negligible differences in output voltage during mechanical deformation, consistent with modeling results (fig. S7). Since the wireless energy transfer is inversely proportional to the coil-to-coil distance (fig. S8), the power harvester resides subcutaneously to maximize the efficiency. Poly(lactic-co-glycolic acid) (PLGA)-based steroid eluting patches release dexamethasone acetate (DMA) over the course of several months (Fig. 2E and fig. S9). The slow rate of dissolution of the bioresorbable conductor (Mo) enables >1 month of functional lifetime under simulated physiological conditions (Fig. 2F and Supplementary Text 4).

A network of skin-interfaced modules placed on various locations of the body acquires diverse data relevant to patient status. These collective data streams form the basis for closed-loop control. As the essential component, the cardiac module mounts on the chest to collect physiological information and to provide RF power to the bioresorbable module. Its materials and architectures (Fig. 2G, fig. S12) follow design principles of soft electronics to ensure robust, irritation-free coupling to the skin (fig. S13) at relevant locations (fig. S14)(19). The multi-haptic module on the mid-medial forearm provides information on patient status and device operation through up to 625 patterns of vibro-tactile input (20). The respiratory module mounts at the suprasternal notch to capture physical activity, body temperature, and respiratory behavior, in a dual-sensing design for accurate operation (21). The hemodynamic module on the forehead measures peripheral blood oxygen saturation (SpO_2)(22).

Fig. 2H shows a block diagram of the transient closed-loop system. An ECG analog front end (AFE) and a microcontroller unit (MCU) in the cardiac module process measured data in real-time to calculate the HR (fig. S15). A BLE-enabled user-interface serves as a control unit that stores and displays ECG tracings and 3-axis acceleration data associated with cardiac and respiratory activity (fig. S16). Fig. 2I-K show that the skin-interfaced modules and data analytics approaches accurately determine HR and respiratory rate (fig. S17). The

hemodynamic module yields SpO_2 comparable to data recorded by a medical-grade finger probe (Fig. 2L). These systems exploit current best practices to protect health data, from the sensor, the BLE link, phone, cloud, and beyond. To ensure secure medical data storage and processing, the interface application is compatible with HTTPS transport layer security (TLS 1.2) and with algorithms for encryption/decryption (fig. S18). In-sensor encryption (AES-128) and HIPAA compliant cloud data storage are available to protect patient data in a HIPPA-compliant manner.

One of the key advances of this transient closed-loop system (10-15) is that the skin-interfaced cardiac module eliminates requirements for wall-plugged, external hardware for power transfer and control of the implanted pacemaker (fig. S19). In vivo studies with a canine whole-heart model demonstrate its capabilities (fig. S20). When the wireless cardiac module generates pulsed alternating currents (6 V_{pp}), the bioresorbable module rectifies the received waveform and delivers it to the myocardium-interface as a cathodic monophasic pulse (~4 mW) (Supplementary Text 5). Investigations using rodent models demonstrate continuous, long-term pacing and biocompatibility (Supplementary Text 6, 7).

An additional feature of this system is in autonomous treatment based on algorithmic identification of ECG signatures of abnormal cardiac activity. For example, hysteresis pacing delivers programmed electrical stimuli if the intrinsic rate falls below a certain threshold, to avoid overriding slow but appropriate intrinsic rhythms (23). Ex vivo human whole heart studies demonstrate this type of treatment for temporary bradycardia (Fig. 3). Anisotropic activation of the membrane potential confirms that the bioresorbable module is the driving source of cardiac activation (Fig. 3C). A flow chart of the feedback control system (Fig. 3D) implemented in the mobile application describes the hysteresis pacing scheme by which the system recognizes bradycardia and activates pacing during the programmed period of treatment. A separate pacing electrode enables manual control of the HR to mimic bradycardia (fig. S40). Fig. 3E shows that the transient closed-loop system detects bradycardia (<54 bpm) and automatically initiates pacing (~100 bpm). After a predetermined pacing duration (10 s), the system automatically stops pacing and evaluates the underlying intrinsic ECG signals to determine the need for additional pacing treatment. When the heart recovers from temporary bradycardia, the system detects the normal HR (~60 bpm) and ceases to deliver on-demand pacing.

For advanced forms of operation, the control module wirelessly communicates with the full collection of skin-interfaced modules via BLE protocols, in a manner that is expandable and customizable to accommodate wide-ranging types of devices with various actuation, feedback and/or monitoring capabilities. The schematic illustration in Fig. 4A and fig. S41 summarizes the most sophisticated system configuration reported here. This network of modules also includes the option to deliver tactile inputs through different patterns of vibration (fig. S42; Movie S1) to inform the patient of the (i) remaining battery life, (ii) proper operation of the cardiac module, (iii) instances of malfunction of the other modules, and (iv) symptoms of bradycardia (Fig. 4B). The haptic module can also be activated to facilitate positioning of the cardiac module during mounting, of particular importance during device replacement to allow for recharging (fig. S43).

Real-time monitoring of cardiopulmonary status and physical activity, along with other essential parameters in a scalable fashion, via comprehensive, multi-modal measurements enables elaborate schemes for rate-adaptive pacing (Supplementary Text 9). Exercise tests of healthy human subjects on stationary bicycles demonstrate this rate-adaptive function (fig. S44). Fig. 4C shows a strong qualitative correlation (i) between measured physical activity and exercise intensity (e.g. rest, slow, fast). The respiratory rate (ii) also correlates to exercise intensity, but the transition is much smoother with some discrepancies. The pacing signal (iii), calculated by (i) and (ii), shows good agreement with the HR of the healthy subject since the metabolic demand is consistent with the level of exercise intensity and respiration. Results from different human subjects (n = 8) confirm the reliability of this algorithm (fig. S46), and Supplementary Text 10 describes strategies for stable and reliable pacing. Other physiological parameters, such as body temperature (iv) and blood oxygen saturation level (v), provide additional information useful for patients with limited cardiopulmonary reserve, slowly resolving pneumonia, or persistent supplemental oxygen requirements post-operatively.

In summary, this transient, closed-loop system represents a class of distributed, wireless bioelectronics technology that provides autonomous electrotherapy over a timeframe that matches post-operative needs through coordinated operation of a network of skin-interfaced modules and a bioresorbable device in time-synchronized communication with a control platform. Data captured from various locations of the body yield detailed information on cardiopulmonary health and physical activity. The results define autonomous, rate-adaptive pacing parameters to match metabolic demand via wireless powering of the bioresorbable module; they also support feedback on device and physiological status via a multi-haptic interface. The bioresorbable module for cardiac pacing undergoes complete dissolution by natural biological processes after a defined operating timeframe. The skin-interfaced devices can be easily removed after patient recovery due to their soft, flexible construction. This system provides a framework for closed-loop technologies to treat various diseases and temporary patient conditions in a way that can complement traditional biomedical devices and pharmacological approaches.

Supplementary Material

Refer to Web version on PubMed Central for supplementary material.

Acknowledgments:

References and Notes

1. Kaszala K, Ellenbogen KA, Circulation. 122, 1328–1340 (2010). [PubMed: 20876446]

2. Hovorka R, Diabet. Med 23, 1–12 (2006).

3. Mickle AD et al., Nature. 565, 361–365 (2019). [PubMed: 30602791]

4. Austin JL, Preis LK, Crampton RS, Beller GA, Martin RP, Am. J. Cardiol 49, 301–306 (1982). [PubMed: 7058746]

5. Lumia FJ, Rios JC, Chest. 64, 604–608 (1973). [PubMed: 4750332]

6. Donovan KD, Lee KY, Anaesth. Intensive Care 13, 63–70 (1985). [PubMed: 3977066]

7. Braun MU et al., PACE - Pacing Clin. Electrophysiol 29, 875–879 (2006). [PubMed: 16923004]

8. McLeod KA, Heart. 96, 1502–1508 (2010). [PubMed: 20813732]

9. Buch E, Boyle NG, Belott PH, Circulation. 123, 378–380 (2011).

10. Choi YS et al., Nat. Biotechnol 39, 1228–1238 (2021). [PubMed: 34183859]

11. Choi YS et al., Nat. Commun 11, 5990 (2020). [PubMed: 33239608]

12. Koo J et al., Sci. Adv 6, eabb1093 (2020). [PubMed: 32923633]

13. Choi YS, Koo J, Rogers JA, MRS Bull. 45, 103–112 (2020).

14. Choi YS et al., Adv. Funct. Mater 30, 2000941 (2020).

15. Kang SK et al., Nature. 530, 71–76 (2016). [PubMed: 26779949]

16. Hwang S-W et al., Science. 337, 1640–1644 (2012). [PubMed: 23019646]

17. Mond HG, Helland JR, Stokes K, Bornzin GA, McVenes R, PACE - Pacing Clin. Electrophysiol 37, 1232–1249 (2014). [PubMed: 25130977]

18. Espe EKS et al., J. Cardiovasc. Magn. Reson 15, 82 (2013). [PubMed: 24034168]

19. Chung HU et al., Nat. Med 26, 418–429 (2020). [PubMed: 32161411]

20. Yu X et al., Nature. 575, 473–479 (2019). [PubMed: 31748722]

21. Jeong H et al., Sci. Adv 7, eabg3092 (2021). [PubMed: 33980495]

22. Rwei AY et al., Proc. Natl. Acad. Sci. U. S. A 117, 31674–31684 (2020). [PubMed: 33257558]

23. García-Izquierdo E, Vilches S, Castro V, Circulation. 135, 711–713 (2017). [PubMed: 28193801]

24. IEEE Standard for Safety Levels with Respect to Human Exposure to Radio Frequency Electromagnetic Fields, 3 kHz to 300 GHz. IEEE Std C95.1-2005 (Revision IEEE Std C95.1-1991) (2006), pp. 1–238.

25. Code for analysis of optical mapping data, (available at https://github.com/optocardiography/RHYTHM-2.0).

26. Code for Masson's trichrome quantification, (available at https://github.com/optocardiography/massonstrichromequantification).

27. Winter KF, Hartmann R, Klinke R, J. Neurosci. Methods 79, 79–85 (1998). [PubMed: 9531463]

28. Dinis H, Colmiais I, Mendes PM, Micromachines. 8, 359 (2017).

29. Pichorim SF, in Proceedings of the14th International Symposium on Biotelemetry (1998), pp. 71–77.

30. Kurs A et al., Science. 317, 83–86 (2007). [PubMed: 17556549]

31. Chung HU et al., Science. 363, 0–13 (2019).

32. U.S. Food and Drug Administration, "Testing and Labeling Medical Devices for Safety in the Magnetic Resonance (MR) Environment: Guidance for Industry and Food and Drug Administration Staff" (2021), (available at https://www.fda.gov/regulatory-information/search-fda-guidance-documents/testing-and-labeling-medical-devices-safety-magnetic-resonance-mr-environment).

33. Guo H et al., Adv. Funct. Mater 31, 2102724 (2021).

34. Yang Q et al., Nat. Mater 20, 1559–1570 (2021). [PubMed: 34326506]

35. Lee G, Choi YS, Yoon H-J, Matter, in press.

36. V Thakor N, Ranjan R, Rajasekhar S, Mower MM, Am. J. Cardiol 79, 36–43 (1997). [PubMed: 9080865]

37. Barsheshet A, Wakslak M, Mower MM, Goldenberg I, Hall B, Ann. noninvasive Electrocardiol 17, 22–27 (2012). [PubMed: 22276625]

38. Thakral A, Stein LH, Shenai M, Gramatikov BI, V Thakor N, J. Appl. Physiol 89, 1159–1164 (2000). [PubMed: 10956364]

39. Kavanagh KM et al., Pacing Clin. Electrophysiol 13, 1268–1276 (1990). [PubMed: 1701542]

40. Force T et al., Circulation. 82, 903–912 (1990). [PubMed: 2394010]

41. Zoll PM et al., Circulation. 71, 937–944 (1985). [PubMed: 3886190]

42. Maisel WH, Rawn JD, Stevenson WG, Ann. Intern. Med 135, 1061–1073 (2001). [PubMed: 11747385]

43. Hwang SW et al., Nano Lett. 15, 2801–2808 (2015). [PubMed: 25706246]

44. Liu K, Tran H, Feig VR, Bao Z, MRS Bull. 45, 96–102 (2020).

45. Leung S-K, Lau C-P, Cardiol. Clin 18, 113–155 (2000). [PubMed: 10709689]

46. Coenen M et al., EP Eur. 10, 327–333 (2008).

47. Dell'Orto S, Valli P, Greco EM, Indian Pacing Electrophysiol. J 4, 137–145 (2004). [PubMed: 16943981]

48. Proietti R et al., Pacing Clin. Electrophysiol 35, 990–998 (2012). [PubMed: 22680238]

49. Palmisano P et al., Eur. Eur. pacing, arrhythmias, Card. Electrophysiol. J. Work. groups Card. pacing, arrhythmias, Card. Cell. Electrophysiol. Eur. Soc. Cardiol 14, 1038–1043 (2012).

50. Krittanawong C et al., Nat. Rev. Cardiol 18, 75–91 (2021). [PubMed: 33037325]
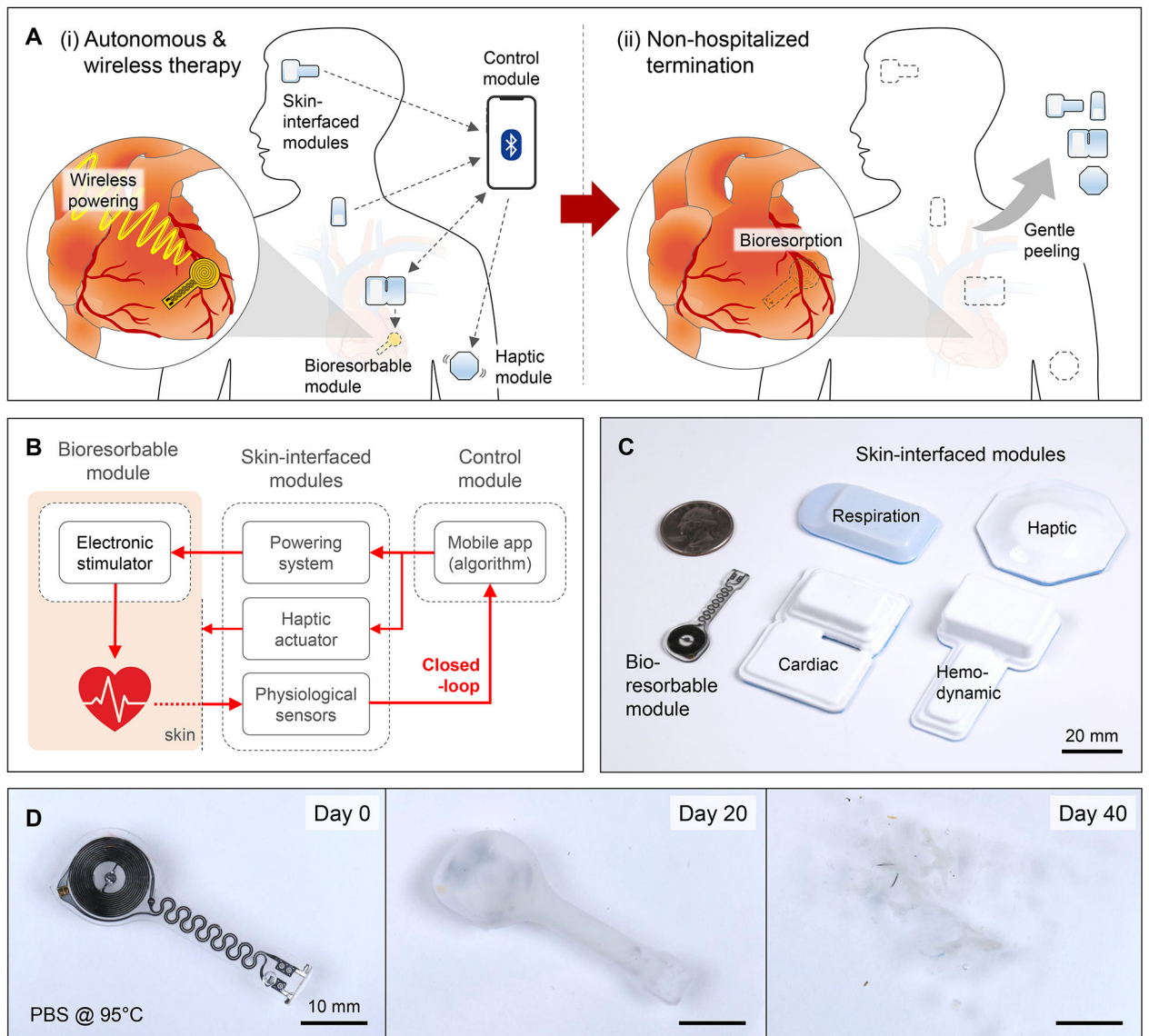
Fig. 1. Transient closed-loop system for temporary cardiac pacing.
(**A**) Schematic illustration of a system for (i) autonomous and wireless pacing therapy and (ii) non-hospitalized termination. (**B**) Operational diagram for continuous monitoring, autonomous treatment, and haptic feedback. (**C**) Photographs showing the sizes of the various modules, relative to a U.S. quarter. (**D**) Photographs of a bioresorbable module at different time points during immersion in a simulated biofluid (PBS; 95 °C).
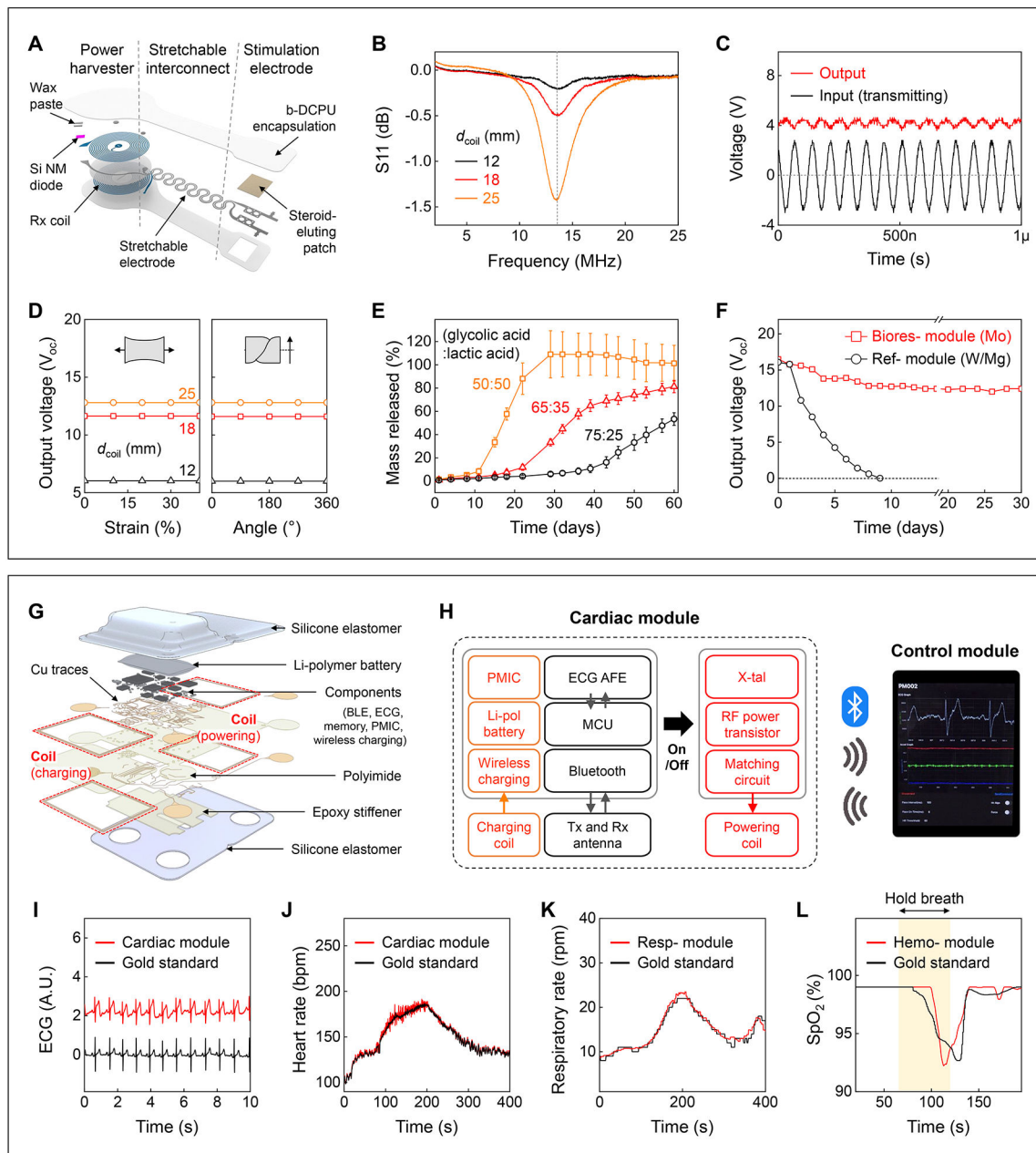
Fig. 2. Materials, design features.
(**A**) Schematic illustration of a bioresorbable module. (**B**) S_{11} values of the Rx coils with different diameters (d_{coil}). (**C**) Example output waveform (red; d_{coil} = 12 mm) wirelessly generated by an alternating current (black; ~3 V_{pp}; 13.56 MHz) applied to the Tx coil. (**D**) Output voltage of devices as a function of tensile strain (left) and twist angle (right) at a fixed transmitting voltage (4 V_{pp}) and frequency (13.56 MHz). (**E**) Drug release behaviors of steroid eluting patches with three different ratios of base polymer. (**F**) Measurements of output voltages of a bioresorbable module (red square, 10 μm thick Mo) and a reference module (black circle, W/Mg with 700 nm / 50 μm thickness) immersed in PBS (37 °C). (**G**) Schematic illustration of a skin-interfaced cardiac module. (**H**) System block diagram
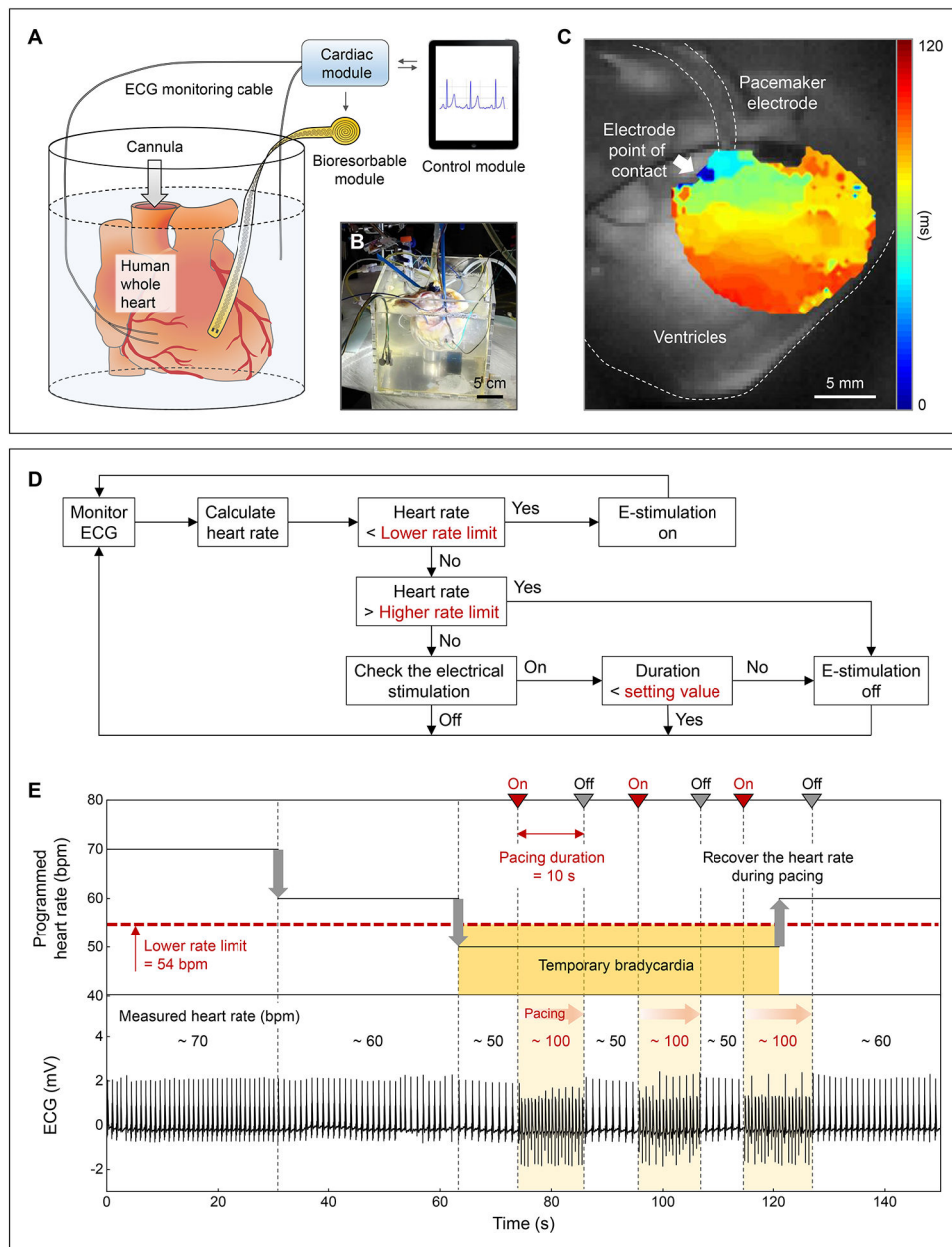
of the cardiac module. PMIC, power management integrated circuit. (**I-L**) Comparisons of ECG, HR, respiratory rate, and SpO_2 level determined by the skin-interfaced modules (red; I, J, cardiac; K, respiratory; L, hemodynamic) and a reference device (black). In L, healthy subject holds breath for 60 s (yellow background).

Fig. 3. Treatment of temporary bradycardia.
(**A**) Schematic illustration and (**B**) photograph of a Langendorff-perfused human whole heart model with a transient closed-loop system (d_{coil} = 25 mm). (**C**) Action potential maps obtained by optical mapping of the human epicardium. (**D**) Flow chart of closed-loop hysteresis pacing to activate the pacemaker upon automatic detection of bradycardia (Supplementary Text 8). (**E**) Programmed HR (top) and measured ECG (bottom) of a human whole heart. Set parameters: lower rate limit, 54 bpm; pacing duration, 10 s; pacing rate, 100 bpm.
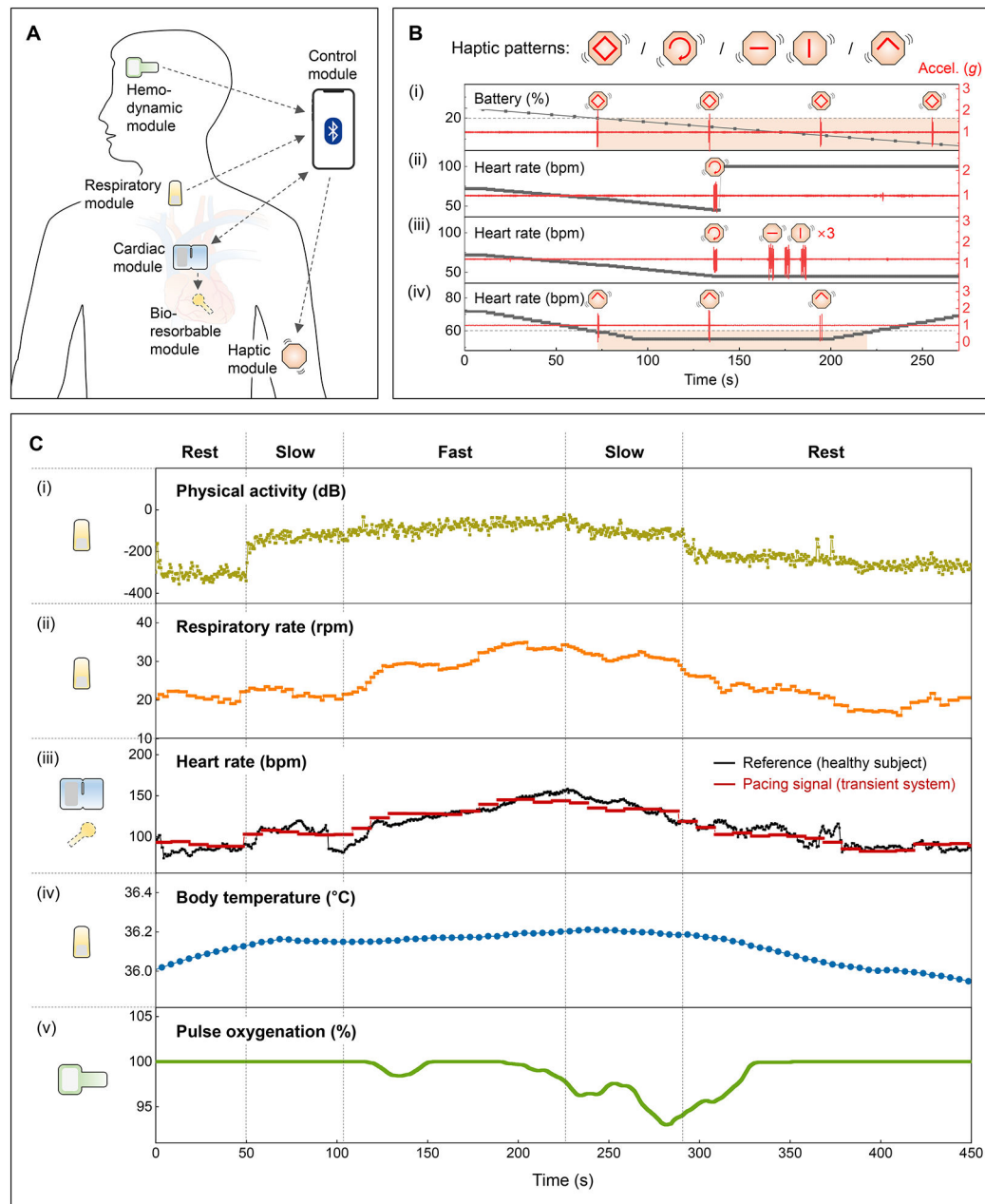
Fig. 4. Patient feedback and adaptive pacing functions.
(**A**) Schematic illustration of a transient closed-loop system. (**B**) Demonstration of the
patient awareness function using a multi-haptic module. Accelerometer data (z-axis)
corresponds to vibrations of the haptic actuators. (**C**) Results of clinical tests with a healthy
human subject. (i) Calculated physical activity and (ii) respiratory rate using data from the
respiratory module. (iii) Comparison of the heart rate (black) of a healthy human subject
monitored by the cardiac module and rate-adaptive pacing signals (red) processed from
the algorithm. (iv) Calibrated and measured changes in core body temperatures using data

from the respiratory module. (v) Representative SpO_2 measurements from the hemodynamic module.